ORIGINAL RESEARCH ARTICLE

Effects of Native AlN Particles on Heterogeneous Nucleation in an Al-3Fe Alloy

ZHONGPING QUE and CHAMINI L. MENDIS

The naturally formed inclusions in an Al-3Fe alloy were investigated using a pressurized melt filtration technique. Naturally formed AlN particles with a rodlike morphology and a size distribution between 200 nm and 4 μm coexist with the native Al_2O_3 particles in the Al-3Fe alloy. These native AlN particles were investigated with scanning electron microscopy (SEM) and high-resolution transmission electron microscopy (HRTEM). A well-defined orientation relationship (OR) between AlN and α-Al was found from the AlN particle embedded in α-Al. A tilt angle of 5.8 deg was observed between {111}α-Al and {0001}AlN at the α-Al/AlN interface. The atomic matching for the α-Al/AlN interface was investigated by considering interfacial segregation on the AlN particles. The heterogeneous nucleation potency of the native AlN particles was investigated. Although these native AlN particles can nucleate the α-Al, the contribution is very small. This contribution reveals the heterogeneous nucleation of α-Al on the native AlN particles and the competitive relationship between the native Al_2O_3 and AlN as the nucleation substrates. The surface modification of the native AlN in Al alloys containing multiple alloy elements and the corresponding effects on the heterogeneous nucleation were preliminarily investigated.

https://doi.org/10.1007/s11661-020-06108-1

I. INTRODUCTION

THE naturally forming inclusions in Al melts were generally considered to be harmful to casting alloys, as these large inclusion films in the melts generate casting defects. With the recent developments in heterogeneous nucleation theory,[1–4] pathways are developed to use these inclusion particles to nucleate α-Al and primary intermetallic phases. Melt conditioning technologies, such as intensive melt shearing,[5, 6] which aims to break the inclusion films and distribute the particles uniformly through the melt, have been developed. The current research on native inoculant use in Al alloys mainly focuses on naturally formed oxides such as α-Al_2O_3, γ-Al_2O_3, $MgAl_2O_4$, and MgO.[7–13] Although other common inclusions, including carbides, borides, nitrides, chlorides, and fluorides, were reported,[14–19] the nucleation potency of these particles in α-Al has not been reported widely. AlN was observed to naturally form in Al-3Fe alloy and coexist with Al_2O_3 particles. The major inoculant in this alloy is α-Al_2O_3 (Mg-free Al alloy). Although AlN was calculated to be not potent for the heterogeneous nucleation of α-Al due to the large misfit between AlN and α-Al,[14] an orientation relationship (OR) was observed between AlN and α-Al in this study, which indicates the possibility of the heterogeneous nucleation.

In the last decades, the progress on the understanding of the grain refinement mechanism of a successful Al-5Ti-1B grain refiner has improved understanding of the heterogenous nucleation.[20–25] The nucleation potency depends on many factors, where the interfacial conditions of the substrates, such as misfit between the solid and substrate, is one of the most important. Recent research shows that the interfacial segregation on nucleation substrates could significantly change the nucleation potency,[20–23] tuning the potency of particles higher or lower. When the alloy melt contains multiple nucleation substrates, the heterogeneous nucleation becomes much more complicated. There is competition among the external grain refiners and the various types of native oxides, even though the competition between the various native oxide particles remains unclear.

In this article, the nature of the native AlN particles was investigated with scanning electron microscopy (SEM) and transmission electron microscopy (TEM). Additionally, the interfacial conditions of AlN, such as interfacial segregation, were investigated based on the OR between the native AlN particles and α-Al. The grain refinement efficiency depends on multiple factors, including particle size, size distribution, and number

ZHONGPING QUE and CHAMINI L. MENDIS are with the Brunel Centre for Advanced Solidification Technology (BCAST), Brunel University London, Uxbridge, Middlesex UB8 3PH, UK. Contact email: Zhongping.Que@brunel.ac.uk

Manuscript submitted July 27, 2020; accepted November 9, 2020.
Article published online December 19, 2020

density of nucleation substrates.[24] For example, although one type of particle in the melt is very potent for the nucleation of α-Al, it may not contribute much to the final grain refinement if there is a low number density of particles or no desirable size distribution.

II. EXPERIMENTAL

The Al-3Fe alloy investigated in this work has a composition of 2.8 pct ± 0.3 pct Fe (all compositions in wt pct). The melting temperature, calculated using the Pandat thermodynamic software with the Scheil model, of this alloy is 701 °C. The starting materials used in this work were commercial purity Al (>99.86 wt pct) and Al-45 wt pct Fe master alloy. The Al-Fe master alloy was added into the pure Al melt and stirred until fully molten. The Al-3Fe alloy melt was prepared at 750 °C in an electric resistance furnace with sufficiently long holding time to ensure the chemical homogeneity of the melt. In order to facilitate direct examination of inclusions, a pressurized melt filtration technique was used on the alloy melt to collect the inclusion particles. The alloy before and after pressurized filtration was cast into a TP1 mold preheated to 380 °C.[26]

Samples for the as-cast microstructural characterization were prepared from the cross section of TP1 samples at the 38-mm height from the bottom, which was solidified at 3.5 K/s.[26] The filtered sample was prepared from the samples collected *via* pressurized filtration to concentrate the inclusion particles following the standard metallographic procedure. The microstructure characteristics of the samples were examined using a Zeiss optical microscope fitted with the Axio Vision 4.3 image analysis system and a Zeiss Supra 35 field emission gun–scanning electron microscope, operated at an accelerating voltage between 5 and 20 kV. To observe the three-dimensional (3-D) morphology of the native particles, the sample was gently etched in 10 vol pct HCl in water for a few seconds and cleaned in ethanol. The filtration materials immediately above the filter were sectioned and prepared for the transmission electron microscopy (TEM) examinations using a Gatan precision ion polishing system. TEM examination was performed on a JEOL* 2100F transmission electron microscope equipped with energy-dispersive X-ray spectroscopy (EDXS) operated at 200 kV. All of the phases investigated in this study were identified using SEM-EDXS and high-resolution TEM (HRTEM) analysis.

*JEOL is a trademark of Japan Electron Optics Ltd., Tokyo.

III. RESULTS

The as-cast microstructure of Al-3Fe solidified at 3.5 K/s was displayed in Figure 1(a). This figure shows that the microstructure consists of primary Fe-containing intermetallic compounds (FIMCs), and the surrounding (α-Al + FIMCs) eutectic, primary α-Al, and surrounding (α-Al + FIMCs) eutectic are displayed. The FIMCs in this sample were identified as θ-$Al_{13}Fe_4$ in both primary and eutectic structures. The magnified image (Figure 1(b)) shows that the primary $Al_{13}Fe_4$ phase has starlike morphology and the associated binary eutectic-$Al_{13}Fe_4$ connected with the primary $Al_{13}Fe_4$ particles. The SEM-backscattered electron (BSE) image

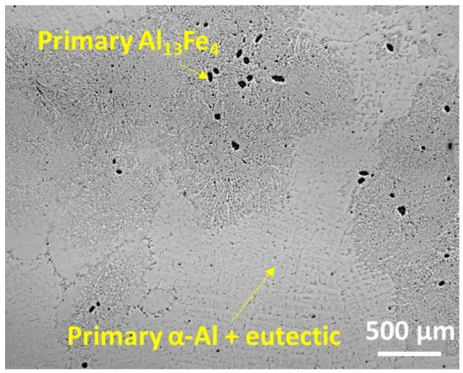

(a)

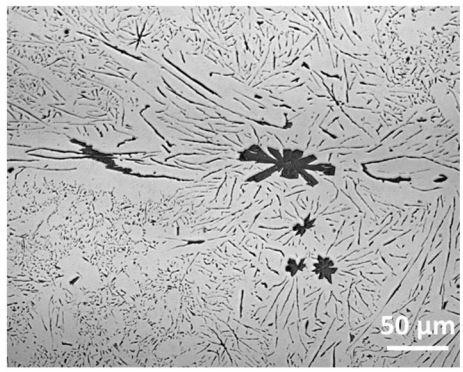

(b)

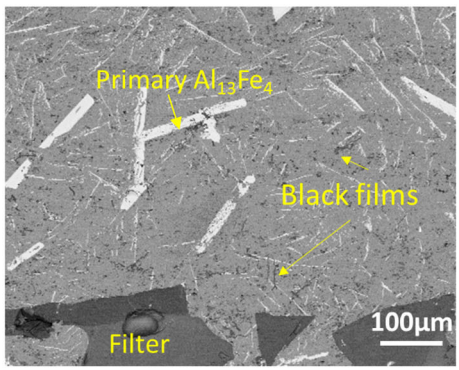

(c)

Fig. 1—(*a*) Optical microstructure of Al-3Fe solidified at 3.5 K/s, showing some primary FIMC particles and some α-Al dendrites with eutectic structure; (*b*) magnified OM image, showing the primary $Al_{13}Fe_4$ particles with the associated ($Al_{13}Fe_4$ + α-Al) eutectic structure; and (*c*) SEM-BSE image of prefill sample above the filter, showing some platelike primary FIMC particles and concentrated oxide films (black).

shown in Figure 1(c) shows the microstructure of the filtered sample just above the filter. The image shows primary platelike and eutectic θ-$Al_{13}Fe_4$ (bright) in the α-Al matrix and large concentration black films identified as native inclusions later. The details of these black films are shown in Figures 2 and 3.

The black films in Figure 1(c) were further observed using SEM with an in-lens detector, and the results are shown in Figures 2 and 3. Figure 2(a) shows the native inclusion particles near porosity in the filtered sample and shows the 3-D morphologies of these inclusion particles. The oxide films (Figure 2(a)) mainly contain compacted and some needlelike particles. The compacted particles identified as Al_2O_3 later have hexagonal morphology with size distribution around 1 μm, and were observed to be associated with the long large $Al_{13}Fe_4$ plates (Figure 2(b)).

The naturally formed inoculant particles collected from the Al-3Fe alloy contained two different types of particles, which were identified as α-Al_2O_3 particles (major) and AlN particles (minor) with SEM with energy-dispersive X-ray analysis and, subsequently, with TEM. Figure 2(a) shows that the major Al_2O_3 particles distribute in most of the oxide films. However, the AlN particles can be observed only along the bifilms, as shown in Figure 3(a). The 3-D morphology of those double films after etching is shown in Figure 3(b) with hexagonal particles at the center of the double films and the long rod particles distributed along the surface. These smaller hexagonal particles and rodlike particles have size distributions from 50 to 200 nm and 200 nm to 4 μm, respectively. The typical SEM-EDXS spectra from both long rods and hexagonal particles are shown in Figures 3(c) and (d), respectively.

The rods mainly contain Al and N with similar atomic fractions of Al and N. The smaller hexagonal particles located in the center of the oxide films contained Al and O, with the amount of O much higher than that of Al. These particles were identified as AlN and α-Al_2O_3 with further TEM analysis. The TEM-EDXS results indicated that the long rods have a composition of N50.2 $\pm$ 0.2 at. pct and Al49.8 $\pm$ 0.2 at. pct. The AlN particles observed in this study have a wider range of sizes than those reported in the pure Al melt.[17]

TEM examination shows that these AlN particles have the hexagonal crystal structure with $a = 3.13 \pm 0.01$ Å, $c = 4.88 \pm 0.01$ Å, and they are (0001) faceted, as illustrated in Figure 4. Most of the AlN particles have no specific in-plane OR with α-Al. However, when AlN particles are embedded in the α-Al grains, these particles have specific OR with α-Al (Figure 5). The interface between AlN and the adjacent α-Al is observed with HRTEM (Figure 5(a)). The indexed selected area electron diffraction (SAED) patterns of both α-Al and AlN are shown in Figures 5(b) and (c), respectively. When the incident electron beam is parallel to [110] of α-Al and $[2\bar{1}\bar{1}0]$ of AlN (Figure 5(a)), the indexed diffraction patterns show an OR between α-Al and AlN as 5.8 deg $(1\bar{1}1)\alpha$-Al//(0001)AlN and the $[110]\alpha$-Al//$[2\bar{1}\bar{1}0]$AlN. This OR provides direct evidence confirming that the *in-situ* AlN particles nucleate α-Al in Al-Fe alloys.

IV. DISCUSSION

A large number density of α-Al_2O_3 was observed as the major native inclusions, and a smaller number density of native AlN particles was observed along the double-side oxide films in an Al-3Fe alloy. The average AlN particle size (~2 μm) is larger than that of α-Al_2O_3 (~200 nm). Most of the AlN particles were distributed along the double films and α-Al_2O_3 particles distributed in the center of the double films. These AlN particles have (0001) terminated planes. The well-defined OR between α-Al and the native AlN particles revealed that the native AlN particles in Al-3Fe can heterogeneously nucleate α-Al.

Fe and Si are common impurities in Al alloys. In this study, the native AlN particles were generated in an Al-3Fe alloy melt that contains Fe and Si as impurities. The solutes or impurities in the melts can segregate to the interface or chemically interact with the surface of substrates to modify the surface condition and then change the heterogeneous nucleation potency.[20–23] For

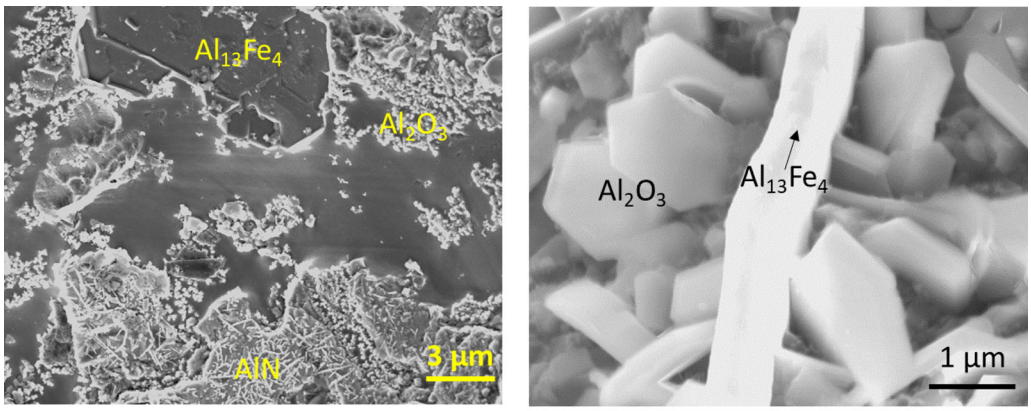

(a) (b)

Fig. 2—SEM analysis with in-lens detector, showing the 3-D morphology of oxide films in the filtered sample: (*a*) a large amount of compacted and needlelike particles and (*b*) compacted particles having hexagonal morphology associated with the $Al_{13}Fe_4$ phase.

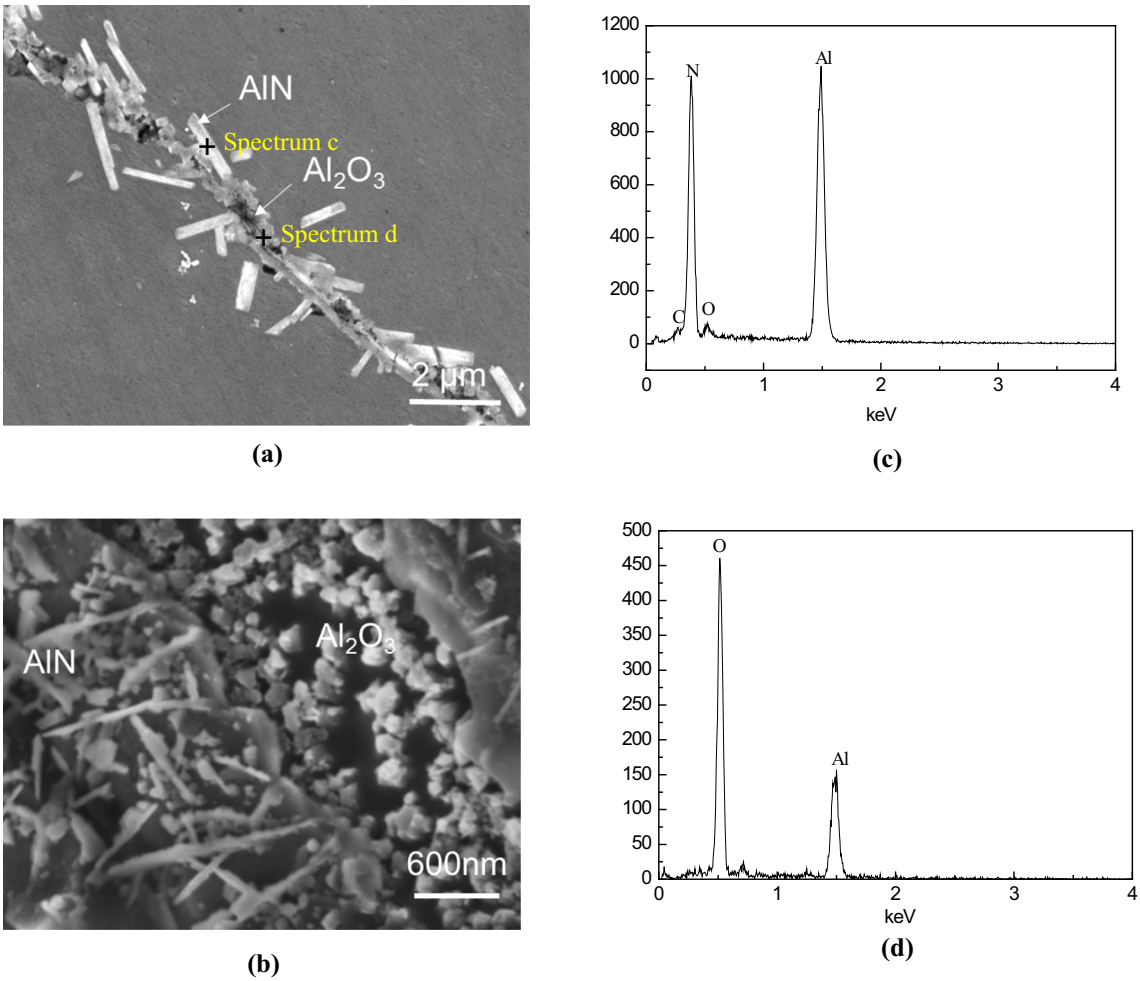

Fig. 3—SEM analysis with in-lens detector of (*a*) the double oxides film, showing some larger long rod particles (AlN) along the film and some smaller particles (Al_2O_3) in the middle of the film; (*b*) 3-D morphology of the double oxide film, showing that the larger particles are in long rod shape and the smaller particles are in hexagonal shape; (*c*) EDXS spectrum, showing that these long rod particles contain Al and N and their ratio is close to Al:N = 1:1; and (*d*) EDXS spectrum, showing that the hexagonal particles mainly contain Al and O.

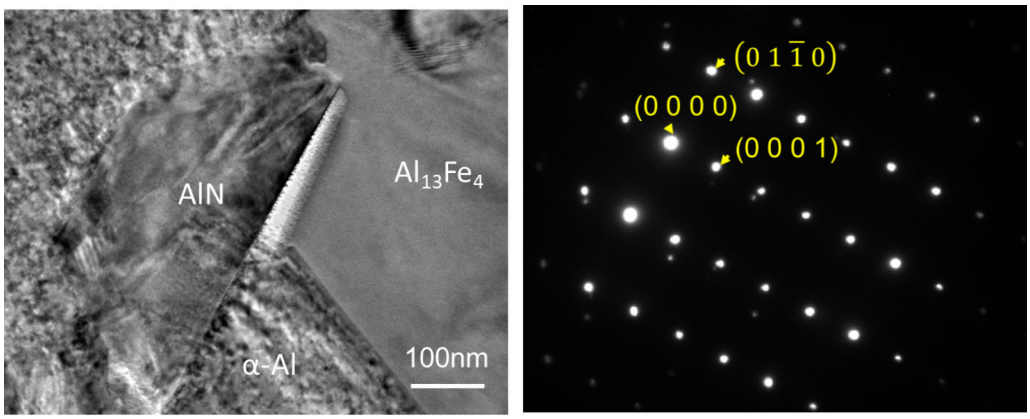

Fig. 4—(*a*) Bright-field TEM image, showing an AlN particle embedded in α-Al matrix and the SAED pattern of (*b*) AlN viewed along the $[2\bar{1}\bar{1}0]$ zone direction, showing that this AlN particle has {0001} faceted planes.

example, the TiB_2 particles with a clean surface are not potent to nucleate α-Al, due to the large misfit between TiB_2 and α-Al. However, the TiB_2 particles in Al-5Ti-1B master alloy refine the α-Al by interacting with the excess Ti, forming Al_3Ti two-dimensional compound (2DC).[20] The latest research shows that this Al_3Ti 2DC

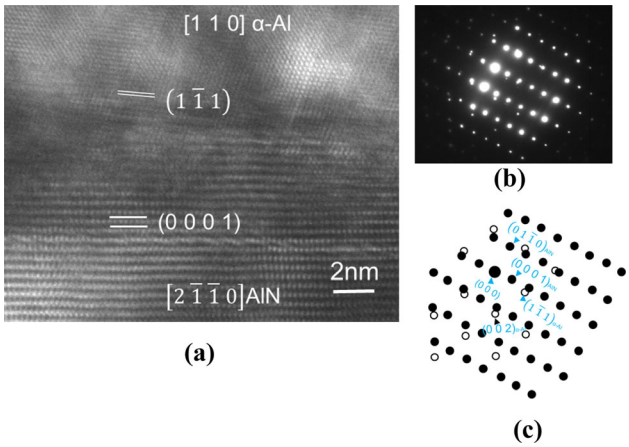

Fig. 5—(*a*) HRTEM image, showing the AlN/α-Al interface with incident electron beam parallel to [110] of α-Al and $[2\bar{1}\bar{1}0]$ of AlN; (*b*) the SAED pattern of AlN and α-Al viewed along the [110] of α-Al and $[2\bar{1}\bar{1}0]$ of AlN; and (*c*) the indexed pattern corresponding to (b), revealing an OR between α-Al and AlN: $(1\bar{1}1)$Al//5.8 deg (0001)AlN and [110]Al//$[2\bar{1}\bar{1}0]$ AlN.

is destroyed by parts per million level Zr addition or higher than 3 wt pct Si.[21, 25] This indicates that the nucleation potency of substrates can be changed significantly by the condition of the interface, such as interfacial segregation or interfacial chemical interaction. These interfacial modifications occur on the wetted externally added particles and also on the naturally formed inclusions. The interfaces in the native inclusions can be even easier to modify due to the better wettability in the melts.

The angle (5.8 deg) between the {111}α-Al and (0001)AlN suggests that the (0001) planes of AlN in this alloy may be modified due to segregation effects. This modification of the interface of AlN could be due to the elemental segregation or chemical interaction with the surface to form ordered atomic layer(s). The real nucleation interface is not $\{111\}_{\alpha\text{-Al}}//(0001)_{\text{AlN}}$, but should be $\left\{\frac{1}{x}\frac{1}{x}1\right\}_{\alpha\text{-Al}}//(0001)_{\text{AlN}}$ considering the tilt angle. Consequently, the OR between α-Al and the native AlN particles in this study could be analyzed as $\left\{\frac{1}{x}\frac{1}{x}1\right\}_{\alpha\text{-Al}}//(0001)_{\text{AlN}}$.

When the tilt angle is 5.8 deg, the parallel plane of α-Al is calculated as $(5\bar{5}4)_{\alpha\text{-Al}}$. Therefore, the real OR between α-Al and AlN is $(5\bar{5}4)_{\alpha\text{-Al}}//(0001)_{\text{AlN}}$ and [110]α-Al//$[2\bar{1}\bar{1}0]$AlN. The misfit between α-Al and AlN was calculated according to the lattice parameters of α-Al and AlN considering the thermal expansion.[27–30] The calculation results show that the misfit between the $(5\bar{5}4)$α-Al and the $(0001)_{\text{AlN}}$ is 1.7 pct, which is much larger than the smallest misfit (0.1 pct) with 1 deg tilt angle. This discrepancy shows that the interface between the α-Al and the native AlN particles might be modified. Here, the lattice mismatch between the $\left\{\frac{1}{x}\frac{1}{x}1\right\}_{\alpha\text{-Al}}$ and modified $(0001)_{\text{AlN}}$ needs to be reconsidered. The misfit calculation in Table I is not suitable for nucleation of solid α-Al and the modified nucleation substrate (AlN). Other factors, such as surface roughness and interfacial segregation, need to be considered to understand the nucleation process in this case.

The comparison of the interfacial atomic matching between the $(111)_{\alpha\text{-Al}}$ on the clean $(0001)_{\text{AlN}}$ and that with interfacial segregation of $(0001)_{\text{AlN}}$ is simulated and is schematically shown in Figure 6. Figures 6(a) and (b) show the simulation results with Crystal Maker software on interface atomic matching. Figure 6(a) shows the atomic matching between the α-Al and the clean $(0001)_{\text{AlN}}$ surface, indicating that the lattice matching is not very good. However, according to the OR of the TEM observation, when the $(5\bar{5}4)_{\alpha\text{-Al}}$ nucleates and templates on the clean surface of the (0001) planes of AlN particles (Figure 6(b)), the coincidence site lattice (CSL) on the atomic templating layers on the AlN surface is very large. According to this simulation, a large number of vacancies will be required at the $(5\bar{5}4)_{\alpha\text{-Al}}//(0001)_{\text{AlN}}$ interface, which is very unlikely.

The segregation of absorbed elements to the surface of AlN to modify the nucleation potency was considered, and the conditions at the interface during the heterogeneous nucleation process were reinvestigated (Figures 6(b) and (d)). In the liquid melts, the Fe solute in Al-Fe alloy and the other impurities, such as Si, can segregate on the surface of AlN particles or have a chemical interaction with the surface atoms of AlN particles. The interfacial segregation of different elements and the atomic radii difference among these segregation elements may generate some defects, such as vacancies at the Al/AlN interface, which might cause a rougher surface on the faceted (0001)AlN. The interfacial segregation and the vacancies on the nucleation substrates change the atomic templating (prenucleation) on the substrates. Therefore, during the nucleation process, the initial templating layers must contain lower numbers of atoms and have larger CSLs for lattice matching, which can be considered as the higher indexed planes of α-Al. After nucleation, the nucleated α-Al continuously grows.[2]

However, as reported,[17] the AlN was considered to not be potent for the heterogeneous nucleation of α-Al. Therefore, the nucleation of α-Al on native AlN particles and its contribution to the final grain refinement need to be further discussed in light of the number density of AlN particles. In liquid, melts containing numbers of different elements might modify all kinds of native inclusions, including AlN and Al_2O_3, which change the nucleation potency in the meantime. Although the TEM results (Figure 5) show direct evidence that the native AlN particles nucleate α-Al, the tilt angle between the AlN and α-Al also indicates that the AlN particles with clean surface may not be potent for the heterogeneous of α-Al.

A nucleus formed during the nucleation stage may not necessarily lead to a grain in the solidified microstructure. According to the grain initiation theory,[31, 32] the nuclei with a radius (r) can only freely grow with a free growth undercoolingΔT_{fg}, where r is the radius of the smallest sphere of the solid phase that engulfs the entire nucleate particle; thus, r equals the largest dimension of

Table I. Lattice Parameters of Oxides and the Misfits between These Oxides and the α-Al

Phase	Thermal Expansion (Temperature (°C))	Crystal Structure	*a*	*c*	Close-Packed Plane	Close-Packed Row	*d*(*hkl*) (nm)	Misfit with α-Al (Pct)
α-Al[24,25]	660	fcc	0.41255	0.41255	{111}	<110>	0.2382	0
AlN[27,28]	666	hexagonal	0.31219	0.49917	{0001}	$2\bar{1}\bar{1}0$	0.4992	− 4.6
α-Al_2O_3	650	hexagonal	0.47789	1.30485	{0001}	$<1\bar{1}00>$	1.3049	− 8.7
γ-Al_2O_3	660	cubic	0.800479	—	{111}	<110>	0.4622	3.1

Table considers all of the lattice parameters with the thermal expansion. The misfit was calculated according to the closed-pack planes of α-Al and the oxides.

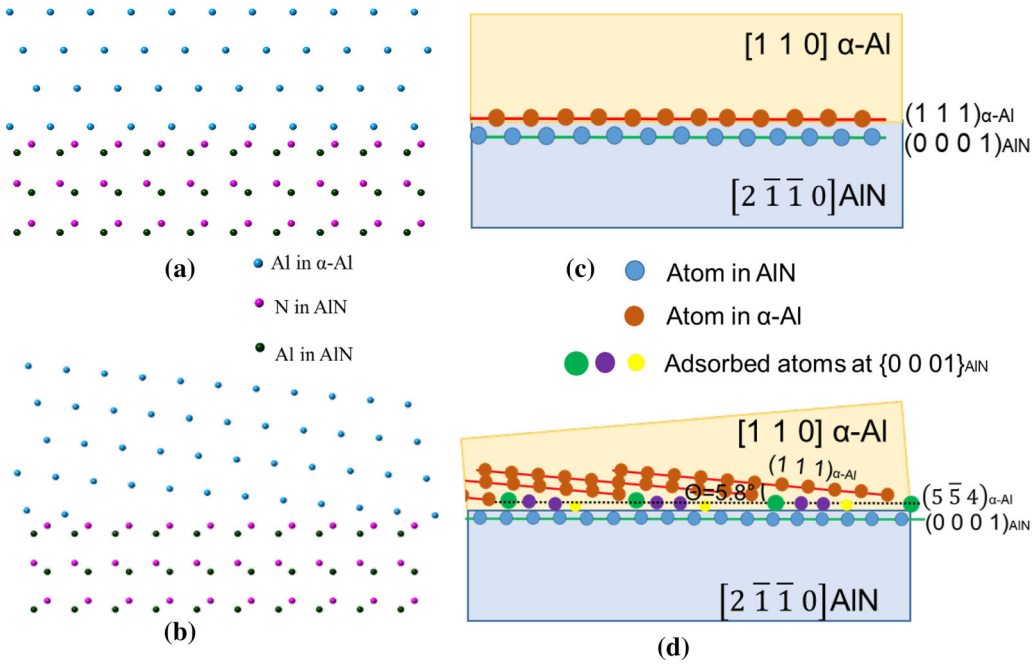

Fig. 6—(*a*) and (*b*) Atomic matching at the interface with Crystal Maker software with the crystal lattice parameters (a) $(1\bar{1}1)[110]$α-Al// $(0001)[2\bar{1}\bar{1}0]$AlN, (b) $(5\bar{5}4)$ [110]α-Al//$(0001)[2\bar{1}\bar{1}0]$ AlN, and (*c*) and (*d*) schematics showing the interfacial atomic matching (c) $(1\bar{1}1)$α-Al on clean (0001)AlN and (d) $(5\bar{5}4)$α-Al nucleated on the (0001)AlN, which has interfacial segregation.

the nucleate particle. Grain initiation is governed by the free growth criterion:[32]

$$\Delta T_{fg} = \frac{2\Gamma}{r}$$

The average size of AlN is much larger than those of the major native Al_2O_3 particles. Therefore, the α-Al grains that nucleated on the larger AlN particles can freely grow more easily than those on the small Al_2O_3 particles. However, due to the very small number density, even if all of the α-Al grains nucleated on the native AlN particles can freely grow, the contribution of AlN particles to the final grain refinement is very small.

Therefore, the nucleation of α-Al on the native AlN particles can be understood from two perspectives. There are at least two types of native inclusion particles, AlN and Al_2O_3, in the Al alloys in this study. These particles compete to work as the nucleation substrate. When these particles have a clean surface, the nucleation potency can be compared according to the calculation of the misfit between these native particles and α-Al (Table I). However, our experimental results show that the surface of these native particles was possibly modified by the interfacial segregation of different types of solute elements in the Al alloys. The nucleation potency became unpredictable. The experimental results show that the native AlN with interfacial modification did nucleate α-Al, which indicated that the AlN particles after interfacial modification became potent for the nucleation of α-Al. However, the number density of AlN is much lower than that of the major Al_2O_3 particles. The AlN can be observed only along the double side films. Therefore, the contribution of AlN particles has little effect on the final grain refinement. However, this study indicates the possibility of the heterogeneous nucleation of α-Al on the native modified AlN particles, which can act as competitive nucleation substrates especially when the casting conditions change.

V. CONCLUSIONS

The main results are summarized as follows. Al_2O_3 was observed as the major oxide in Al-3Fe alloy. The AlN particles, which have long rod morphology and sizes between 200 nm and 4 μm, naturally form in Al-3Fe alloy and distribute along the double oxide films. A well-defined OR between α-Al and AlN was observed as $(1\bar{1}1)$Al//5.8 deg (0001)AlN and [110]Al//$[2\bar{1}\bar{1}0]$ AlN. The nucleation potencies of Al_2O_3 and AlN for different phases, such as $Al_{13}Fe_4$ and α-Al, are changed and become unpredictable due to the interfacial segregation. Therefore, the AlN particles in some bifilms are possible to nucleate α-Al. However, the nucleation rate of the Al on the native AlN is very low due to the low number density of agglomeration bifilms. Therefore, the contribution of native AlN to the grain refinement is very limited.

ACKNOWLEDGMENTS

The Engineering and Physical Sciences Research Council (EPSRC) is gratefully acknowledged for providing financial support under Grant No. EP/N007638/1. The Experimental Techniques Centre (ETC), Brunel University, is acknowledged for providing access to SEM and TEM facilities.

OPEN ACCESS

REFERENCES

1. Z. Fan: *Metall. Mater. Trans. A*, 2013, vol. 44A, pp. 1409–18.
2. C.M. Fang, H. Men, and Z. Fan: *Metall. Mater. Trans. A*, 2018, vol. 49A, pp. 6231–42.
3. H. Men and Z. Fan: *Metall. Mater. Trans. A*, 2018, vol. 49A, pp. 2766–77.
4. C.M. Fang and Z. Fan: *Comput. Mater. Sci.*, 2020, vol. 171, p. 109258.
5. Z. Fan, Y. Wang, Z.F. Zhang, M. Xia, H.T. Li, J. Xu, L. Granasy, and G.M. Scamans: *Int. J. Cast Met. Res.*, 2009, vol. 22 (1–4), pp. 318–22.
6. Z. Fan, B. Jiang, and Y. Zuo: U.S. Patent 9,498,820, B2, 2016.
7. Q. Chen: Ph.D. Thesis, University of Birmingham, Birmingham, England, 2016.
8. S. Impey, D.J. Stephenson, and J.R. Nicholls: *Int. Conf. on the Microscopy of Oxidation*, University of Cambridge, Cambridge, UK, 1990, pp. 238–44.
9. M. Silva and D. Talbot: *Essential Readings in Light Metals*, vol. 3, *Cast Shop for Aluminum Production*, 2013, p. 137.
10. D.L. Belitskus: *Oxid. Met.*, 1974, vol. 8 (5), pp. 303–07.
11. I. Haginoya and T. Fukusako: *Trans. Jpn. Inst. Met.*, 1983, vol. 24 (9), pp. 613–19.
12. O. Salas, H. Ni, V. Jayaram, K.C. Vlach, and C.G. Levi: *Mater. Res.*, 1991, vol. 6 (09), pp. 1964–81.
13. H.-T. Li, Y. Wang, and Z. Fan: *Acta Mater.*, 2012, vol. 60 (4), pp. 1528–37.
14. C.J. Simensen and C. Berg: *Alum. Dusseldorf*, 1980, vol. 56, pp. 335–40.
15. K.L. More, P.F. Tortorelli, L.R. Walker, J. Hryn, and G. Krumdick: *Mater. High Temp.*, 2003, vol. 20, pp. 453–60.
16. C. Borgonovo and M.M. Makhlouf: *Metall. Mater. Trans. A*, 2016, vol. 47A, pp. 1818–27.
17. F. Wang and Z. Fan: *Metall. Mater. Trans. A*, 2019, vol. 50A, pp. 2519–26.
18. W.D. Griffiths and R. Raiszadeh: *J. Mater. Sci.*, 2009, vol. 44, pp. 3402–07.
19. R. Raiszadeh and W.D. Griffiths: *Metall. Mater. Trans. B*, 2006, vol. 37B, pp. 865–71.
20. Z. Fan, Y. Wang, Y. Zhang, T. Qin, X.R. Zhou, G.E. Thompson, T. Pennycook, and T. Hashimoto: *Acta Mater.*, 2015, vol. 84, pp. 292–304.
21. Y. Wang, C.M. Fang, L. Zhou, T. Hashimoto, X. Zhou, Q.M. Ramasse, and Z. Fan: *Acta Mater.*, 2019, vol. 164, pp. 428–39.
22. Z.P. Que, Y.P. Zhou, Y. Wang, and Z. Fan: *Solidification Processing Conf.*, 2017, pp. 158–61.
23. Y. Wang, Z.P. Que, Y. Zhang, and Z. Fan: *Solidification Processing Conf.*, 2017, pp. 56–60.
24. Z. Fan, F. Gao, B. Jiang, and Z.P. Que: *Sci. Rep.*, 2020, vol. 10, p. 9448.
25. Y. Li, B. Hu, B. Liu, A. Nie, Q. Gu, J. Wang, and Q. Li: *Acta Mater.*, 2020, vol. 187, pp. 51–65.
26. Aluminium Association: Standard Test Procedure for Aluminium Alloy Grain Refiners: TP-1, Washington, DC, 1987.
27. A.S. Cooper: *Acta Cryst.*, 1962, vol. 15, pp. 578–82.
28. W. John: *Arblaster: Selected Values of the Crystallographic Properties of Elements*, Cleveland, OH, ASM International, 2018, p. 129.
29. H. Schulz and K.H. Thiemann: *Solid State Commun.*, 1977, vol. 23, pp. 815–19.
30. W.M. Yim and R.J. Paff: *J. Appl. Phys.*, 1974, vol. 45, pp. 1456–57.
31. A.L. Greer and T.E. Quested: *Philos. Mag.*, 2006, vol. 86, pp. 3665–80.
32. T.E. Quested and A.L. Greer: *Acta Mater.*, 2004, vol. 52 (13), pp. 3859–68.